Journal of Power Sources 240 (2013) 589–597

Contents lists available at SciVerse ScienceDirect

Journal of Power Sources

journal homepage: www.elsevier.com/locate/jpowsour

Ni–P and Ni–Mo–P modified aluminium alloy 6061 as bipolar plate material for proton exchange membrane fuel cells

Amani E. Fetohi [a], R.M. Abdel Hameed [b,*], K.M. El-Khatib [a]

[a] Chem. Eng. & Pilot Plant Dept., National Research Center, Dokki, Giza, Egypt
[b] Chemistry Department, Faculty of Science, Cairo University, Giza, Egypt

HIGHLIGHTS

- Aluminium alloy 6061 was coated with Ni–P and Ni–Mo–P.
- Lowered I_{corr} values were obtained at Ni–P and Ni–Mo–P coated AA6061.
- Ni–P/AA6061 was more stable than Ni–Mo–P/AA6061 after 40 min in potentiostatic polarization test.
- Ni–P and Ni–Mo–P coated AA6061 showed lowered ICR values.

GRAPHICAL ABSTRACT

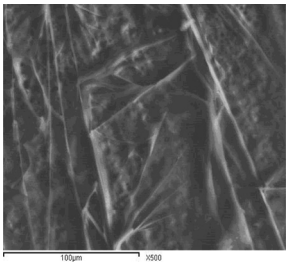

ARTICLE INFO

Article history:
Received 5 January 2013
Received in revised form
6 April 2013
Accepted 16 April 2013
Available online 28 April 2013

Keywords:
Bipolar plate
Polymer electrolyte membrane fuel cells
Nickel–phosphorous
Nickel–molybdenum–phosphorous
Potentiodynamic polarization technique

ABSTRACT

Aluminium alloy 6061 (AA6061) is coated with Ni–P and Ni–Mo–P using electroless and electroplating techniques. Coated substrates were characterized using scanning electron microscopy and energy dispersive X-ray analysis. Potentiodynamic polarization technique is applied to investigate the corrosion resistance characteristics of coated AA6061 in (0.5 M H_2SO_4 + 2 ppm HF) solution. Coating AA6061 with Ni–P and Ni–Mo–P shifts its corrosion potential towards more positive values and lowers the corresponding current density values. The stability of prepared coatings under simulated cathode condition in PEM fuel cells is tested in air-saturated solution at +160 mV versus (mercury/mercury sulphate electrode (MMS)) for 5 h. After 40 min from starting the polarization test, Ni–P coating is found to be more stable than Ni–Mo–P. Ni–P and Ni–Mo–P coated AA6061 show a lowered ICR value at a compaction force of 140 N cm^{-2} by 2.22 and 1.88 times, respectively when compared to bare aluminium alloy.

1. Introduction

Proton exchange membrane fuel cells (PEMFCs) are environmentally friendly power sources due to their high power density, fast start-up and low operating temperature. However, large-scale commercialization of PEMFCs is prohibited by their increased cost, weight and volume [1]. In PEM fuel cells, bipolar plates account for 70% of the stack weight and 60% of its cost [2,3]. There are three main categories of bipolar plate materials; namely: carbon–carbon composites, carbon–polymer composites and metals [4].

Aluminium represents a suitable bipolar plate material in polymer electrolyte membrane fuel cell applications because of its low density, low fabrication cost, light weight and high specific strength and rigidity [5,6]. However, the corrosion resistance of Al and its alloys is affected by the raised temperature (65–90 °C), acidic (pH 2–3) and humid environment. This corrosion of bipolar plates would release metallic ions with migration towards both catalyst layers and polymeric membrane to degrade the performance of fuel cells [7]. Moreover, the formation of passive oxide

* Corresponding author. Tel.: +20 1145565646; fax: +20 235727556.
E-mail addresses: randa311eg@yahoo.com, noura31176@hotmail.com (R.M. Abdel Hameed).

0378-7753/$ – see front matter © 2013 Elsevier B.V. All rights reserved.
http://dx.doi.org/10.1016/j.jpowsour.2013.04.085

layers on Al surfaces increases its interfacial contact resistance [8]. Therefore, protective coating layers are adopted to avoid corrosion. Coatings should have good electrical conductivity with a value of the thermal expansion coefficient similar to that of the metal substrate. They should also adhere to the base metal to prevent its corrosion in the acidic media [9]. The coating materials are either carbon-based or metal-based [9,10]. The carbon-based coatings include graphite, conductive polymers, diamond like carbon and organic self-assembled polymers [11]. On the other hand, the metal-based coating consists of metal nitrides [12–16] and metal carbides [17].

Parallel to the development of a corrosion resistant metallic material, it is also necessary to adopt an efficient and cost effective fabrication process of the bipolar plate in order to make the production of metallic bipolar plates commercially viable. The painted polyaniline on AA6061 aluminium surface showed a reduced corrosion current by one order of magnitude with only a minor increase in contact resistance [18]. Potentiodynamic polarization curves of aluminium substrate coated with chromium nitride by magnetron sputtering showed much lower susceptibility to pitting corrosion in 3.5% NaCl solution at room temperature with an increased corrosion resistance with respect to uncoated samples [19].

It is well established that the molybdenum metal is corrosion resistant as many valve metals due to the formation of a passive layer on its surface in aqueous environments [20–25]. Badawy and Al-Kharafi [26] have investigated the corrosion and passivation behaviours of molybdenum in aqueous solutions. The electrochemical impedance spectroscopy and polarization measurements have shown that the naturally occurring passive film at molybdenum surface is more stable in acidic than in alkaline solutions. In basic solutions, the stability of the passive film decreases due to the formation of soluble species ($HMoO_4^-$ and MoO_4^{-2}). It is turned out that the activation energy of oxide film dissolution is lower in basic solutions (128.3 kJ mol^{-1}) than in neutral (152.5 kJ mol^{-1}) or acidic solutions (162.4 kJ mol^{-1}) which reflects the relative instability of the passive film in basic solutions. The molybdenum oxide film was found to catalyze the electro-reduction of chlorate and bromate in H_2SO_4 solution [27]. It also displayed a catalytic activity towards a large number of redox species comprising a wide range of formal potentials and various charges including a standard redox couple, ferrocene and its derivatives [28].

Ni–P coatings are widely used in the mechanical, chemical and electronic industries because of their unique corrosion and wear resistance [29]. The physical and chemical properties of Ni–P deposits were improved by alloying with a third metal such as Zn, Cu, Co, Fe, Sn, W, Mo, etc [30–32]. Coating Al alloy 5251 [33] and Al alloy 1050 [34] with Ni–Co–P deposit using electroplating power supply technique lowers their corrosion current densities and shifts the corrosion potential towards more noble values. SEM images confirmed the formation of agglomerates of Ni–Mo–P particles on Al_2O_3 by applying the incipient wetness impregnation method [35]. They exhibit better thermal stability and superior long-term corrosion resistance than Ni–P [36,37]. Moreover, Ni–Mo–P coatings on aluminium surface showed ICR values that exceed the U.S. DOE's target [38].

In this study, electroless and electroplating techniques were applied to coat AA6061 with Ni–P and Ni–Mo–P. Their surface morphology was imaged using scanning electron microscopy (SEM) analysis, while energy dispersive X-ray (EDX) technique could determine the chemical composition of these formed coatings. The corrosion resistance was examined using Tafel plots and potentiostatic polarization tests. The interfacial contact resistance of coated AA6061 substrate was also measured at different compression pressures.

2. Experimental

2.1. Electrode preparation

A rod of AA6061 was fixed inside a glass tube by means of epoxy resin. The resulting disk-shaped electrode with apparent surface area of 0.1 cm^2 was pretreated by polishing with emery papers in different grades. Its surface was finally cleaned by triply distilled water, followed by rinsing with acetone. The chemical composition of AA6061 was presented in Table 1.

2.2. Zincating process

Zincating pretreatment was carried out prior to metal plating on Al to remove its surface insulating oxide film. Dipping Al substrate in the zincating solution would dissolve its oxide layer and a part of the surface. Zn metal was then deposited [39–41]. Tang et al. [42] found that the zincating process significantly improves the corrosion resistance of Ni–P coating as evidenced by slight E_{corr} increase and significant I_{corr} decrease. Briefly, Al alloy surface was immersed in acetone for 30 s, followed by acid stripping in 1 M H_2SO_4 solution for 10 s. The zincating process requires the immersion of AA6061 in (200 g NaOH + 10 g ZnO) dissolved in 1 L H_2O for 20 s. This step was repeated after cleaning Al substrate in deionized water and 1 M H_2SO_4 solution, each one for 10 s.

2.3. Coating process

The bath composition of the plating solutions is listed in Table 2. $NiSO_4 \cdot 6H_2O$ and $Na_2MoO_4 \cdot 2H_2O$ were used as the precursor salts of nickel and molybdenum, respectively. The reduction step was performed by adding sodium hypophosphite that also deposits P metal. Sodium citrate was used as a complexing agent. Sodium molybdate is added to the plating bath in certain amounts to prepare Ni–Mo–P coatings with Ni:Mo molar ratios of 1:0.33 and 1:0.50.

AA6061 was coated with Ni–P and Ni–Mo–P using electroless and electroplating techniques. The electroless deposition was carried out for 20 min at 70–90 °C. On the other hand, the electroplating process was operated at 6 V for 7 min. Two-electrodes circuit was built to electroplate Al alloy using power supply technique. The working electrode was zincated AA6061, while Pt wire was the counter electrode. A third electrode [Hg/Hg_2SO_4/1.0 M H_2SO_4(MMS)] was added when AA6061 substrate was coated by chronoamperometry technique. Two Ni:Mo molar ratios were assigned during bath preparation as 1:0.33 and 1:0.50 to form Ni–Mo–P (1:0.33)/AA6061 and Ni–Mo–P (1:0.5)/AA6061 substrates, respectively.

2.4. Physical characterization of the prepared coatings

The surface morphology of AA6061 was scanned before and after coating with Ni–P and Ni–Mo–P deposits using the scanning electron microscopy. After potentiostatic polarization test for long time, the morphology changes in the substrate surfaces were also scanned. The used scanning electron microscope was JXA–840A, Electron Probe Microanalyzer, JEOL, Japan. It is equipped with EDX analysis "INCA X-sight, OXFORD instruments, England" unit to determine the chemical composition of the coatings.

Table 1
Chemical composition of AA6061.

Element	Zn	Mg	Mn	Cu	Fe	Si	Ti	Cr
Weight%	0.25	0.80–1.20	0.15	0.15–0.40	0.70	0.40–0.80	0.15	0.04–0.35

Table 2
Composition of plating baths of Ni–P and Ni–Mo–P coatings on AA6061.

Composition	Ni–P	Ni–Mo–P	
		Ni:Mo	Ni:Mo
		1:0.33	1:0.50
$NiSO_4 \cdot 6H_2O$/g l^{-1}	30	30	30
$Na_2MoO_4 \cdot 2H_2O$/g l^{-1}	–	10	15
$NaH_2PO_2 \cdot H_2O$/g l^{-1}	20	20	20
$C_6H_5Na_3O_7 \cdot 2H_2O$/g l^{-1}	20	20	20
Temperature/°C	70–80	85–90	85–90
pH	5.70	6.68	6.80

2.5. Corrosion measurements

Voltalab6 Potentiostat driven by a PC for data processing was used to study the corrosion performance of bare AA6061 and as-deposited Ni–P and Ni–Mo–P coatings. Corrosion parameters were calculated from potentiodynamic polarization curves. A conventional three-electrode cell is constructed. Corrosion measurements were tested in a simulated environment of PEM fuel cell [(0.5 M H_2SO_4 + 2 ppm HF) solution] at room temperature without any gas purging. The working electrode was immersed in this solution and left until the steady-state open circuit potential was attained. It was taken as the free corrosion potential ($E_{i=0}$). Thereafter, Tafel measurements were recorded at a scan rate of 1 mV s^{-1}, starting from −250 mV with respect to $E_{i=0}$ up to 1000 mV versus mercury sulphate reference electrode.

2.6. Interfacial contact resistance measurements

Wang et al. [43] have described how to measure the interfacial contact resistance values between coated AA6061 substrate and the gas diffusion layer. Flexible and nonwoven gas diffusion layer (LyFlex™), manufactured by Lydall Inc. was used. Our earlier work showed the used setup [33,34]. Coated AA6061 substrate was sandwiched between two carbon papers and then enveloped between two gold-plated copper plates using a stem with a surface area of 1.0 cm^2. A gradual increase in the compaction force was applied while a constant electric current of 1.0 A was passed. The resulting potential difference across the cell was recorded. The surface resistivity of coated AA6061 substrates was calculated using Ohm's law. Interfacial contact resistance values could be then estimated using the following equation:

$$\mathrm{ICR} = A \times (R - R_{cp})/2$$

where: R_{cp} is the resistivity contribution by the carbon paper/gold-plated copper plate interface; R is the resistivity contribution by the carbon paper/gold-plated copper plate interface/coated aluminium substrate and A is the sample surface area.

3. Results and discussion

3.1. SEM and EDX analyses of coated AA6061 samples

The scanning electron micrographs of Ni–Mo–P (1:0.33)/AA6061 substrates, formed by different deposition techniques, were represented in Fig. 1. Irrespective of the deposition technique, a coarse Ni–Mo–P coating layer was formed containing many cracks. These observed cracks may be probably induced by the release of internal stresses generated by the adsorption–desorption processes involved in the redox reactions and phosphorous codeposition that alter the crystallographic structure of nickel [44]. Bright deposits of nickel were observed in Fig. 1(a) and (b). They

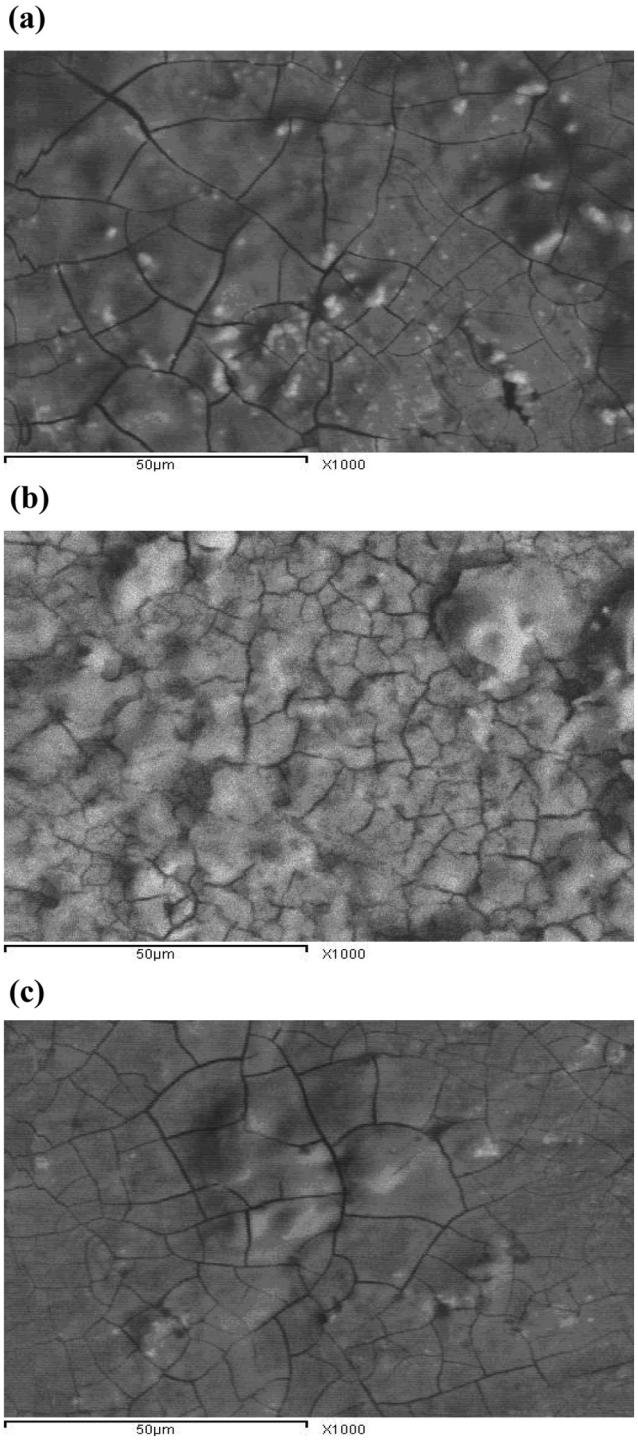

Fig. 1. Scanning electron micrographs of AA6061 coated with Ni–Mo–P (1:0.33) formed by (a) electroless and electroplating [(b) power supply and (c) chronoamperometry] techniques.

were homogeneously distributed on coated AA6061 surface formed by electroplating power supply technique [Fig. 1(b)], compared to localized deposits at the one formed by electroless method [Fig. 1(a)]. AA6061 coated with electroplating chronoamperometry technique contains less nickel deposits [Fig. 1(c)].

Electroplating power supply technique was applied to coat AA6061 with Ni–P and Ni–Mo–P in Ni:Mo molar ratio of 1:0.5. Their surface morphologies were shown in Fig. 2. Ni–P coating appears in Fig. 2(a) as a spongy structure with grooves in different

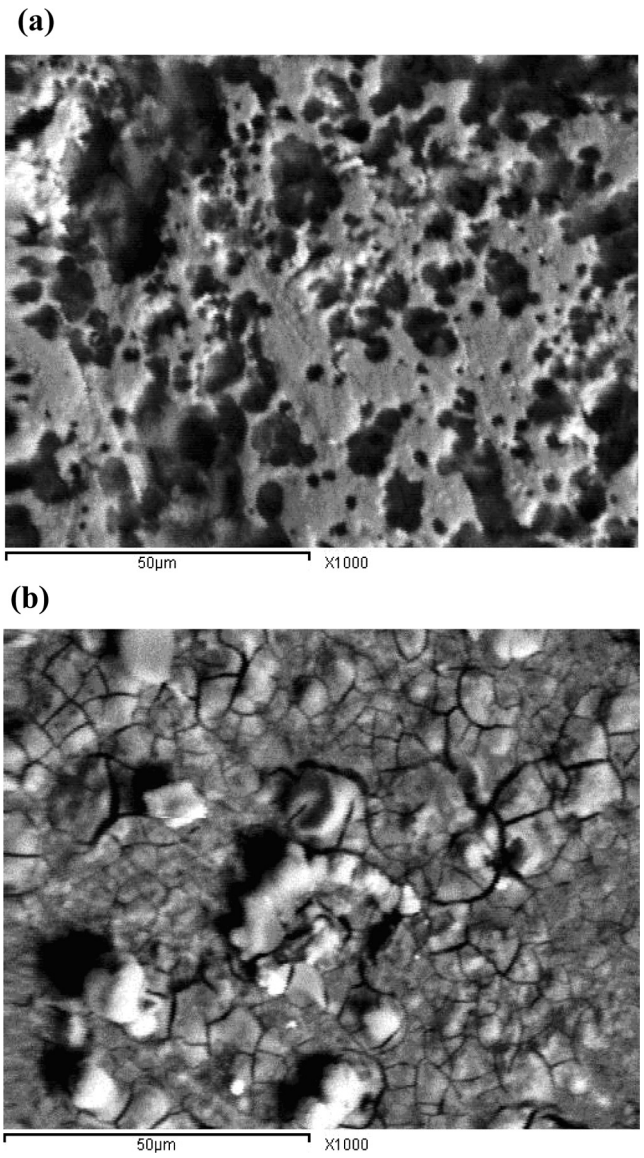

Fig. 2. Scanning electron micrographs of AA6061 coated with (a) Ni–P and (b) Ni–Mo–P (1:0.5) formed by electroplating power supply technique.

sizes. Ramified cracks are widely distributed throughout Ni–Mo–P (1:0.5) deposit on AA6061 surface in Fig. 2(b). As observed for the surface morphology of Ni–Mo–P (1:0.33) deposit, formed by electroplating power supply technique in Fig. 1(b), nickel was homogeneously covering the whole coating with the formation of large deposit aggregates.

The chemical composition of Ni–Mo–P (1:0.33)/AA6061, formed by different deposition techniques, was determined using energy dispersive X-ray analysis. The corresponding weight and atomic percentages of the chemical components of each coating are listed in Table 3. Sodium, sulfur and zinc were recorded after the substrate pretreatment. The weight percentage of phosphorous is altered in Ni–Mo–P (1:0.33) coating according to its formation method. The coated substrate formed by electroless plating contains the highest deposited amount of P [9.72%]. This high phosphorous percentage confirms the formation of an amorphous structure [45]. On the other hand, the lowest phosphorous weight percentage [3.69%] was observed in the coating formed by electroplating power supply technique. Coated aluminium alloy 5251 [AA5251] with Ni–Co–P [with Ni:Co molar ratio of 1:1] by electroless and electroplating techniques, obeyed the same ordering of the phosphorous content [33]. When the atomic percentage of molybdenum is compared to that of nickel in Ni–Mo–P (1:0.33)/AA6061, it could be arranged in an ascending order based on the formation method as follows: electroplating power supply [0.15:1] < electroplating chronoamperometry [0.74:1] < electroless [1.39:1]. The weight percentage of deposited nickel in Ni–Mo–P (1:0.33)/AA6061 was also altered based on the formation method [electroplating chronoamperometry (3.78%) < electroless (10.22%) < electroplating power supply (21.97%)]. This order agreed with the nickel particles density in SEM images in Fig. 1. The chemical composition of Ni–P and Ni–Mo–P (1:0.5) coatings, formed by electroplating power supply technique, was also listed in Table 4. It was observed that when adding Na_2MoO_4 to the deposition solution, a decreased amount of phosphorous in the coating is formed. This is apparent from the increased amount of P in Ni–P coating [13.34%], compared to 3.69% and 1.78% when Ni:Mo molar ratio in the deposition solution is 1:0.33 and 1:0.5, respectively. Bai et al. [38] concluded that increasing Na_2MoO_4 concentration in the plating bath would increase MoO_4^{-2} adsorption on the substrate surface. This would retard the oxidation of $H_2PO_2^-$, resulting in a decreased deposited amount of phosphorous [36,37]. The catalytic reduction reaction of nickel was also slowed down to decrease the overall deposition rate of Ni–Mo–P alloy. This is confirmed by calculating the total weight percentages of nickel, molybdenum and phosphorous in Ni–P, Ni–Mo–P (1:0.33) and Ni–Mo–P (1:0.5) coatings as 84.52%, 30.36% and 12.81%, respectively.

3.2. Corrosion behaviour of coated AA6061 substrates

Potentiodynamic polarization curves of AA6061 substrate before and after its coating with Ni–P and Ni–Mo–P using different deposition methods in (0.5 M H_2SO_4 + 2 ppm HF) solution were studied at 25 °C. Fig. 3 shows Tafel plots of bare and coated AA6061 substrates using electroplating power supply technique. The corresponding electrochemical corrosion parameters estimated from

Table 3
Chemical composition of AA6061 coated with Ni–Mo–P (1:0.33) (according to EDX analysis). The coating was formed by different deposition techniques.

Element	Deposition technique					
	Electroplating				Electroless plating	
	By chronoamperometry		By power supply			
	Weight%	Atomic%	Weight%	Atomic%	Weight%	Atomic%
Na K	5.16	6.50	9.11	13.62	16.63	28.64
Al K	73.53	79.02	46.23	58.98	17.67	25.94
P K	7.27	6.80	3.69	4.07	9.72	12.42
S K	4.12	3.73	2.02	2.13	4.54	5.61
Mo K	4.56	1.38	4.70	1.92	23.16	9.56
Ni K	3.78	1.87	21.97	12.85	10.22	6.89
Zn K	1.58	0.70	12.28	6.43	18.06	10.94

Table 4
Chemical composition of AA6061 coated with Ni–P and Ni–Mo–P (1:0.5) (according to EDX analysis). The coatings were formed by electroplating power supply technique.

Element	Ni–P		Ni–Mo–P (1:0.5)	
	Weight%	Atomic%	Weight%	Atomic%
Na K	1.95	4.11	2.59	3.49
Al K	11.45	19.70	76.95	85.97
P K	13.34	19.18	1.78	1.75
S K	1.00	0.98	0.85	0.93
Mo K	–	–	2.27	0.88
Ni K	71.18	55.15	8.76	4.55
Zn K	1.08	0.88	6.80	2.43

Tafel plots are recorded in Table 5. Compared to E_{corr} value of bare AA6061 substrate [−1056 mV], more positive corrosion potentials were shown by Ni–P and Ni–Mo–P coated AA6061 substrates formed by different deposition techniques. In general, it was observed that, adding molybdenum to the deposition bath shifted E_{corr} of the formed coated substrates towards more positive values. However, the presence of increased amount of molybdenum [for baths containing Ni:Mo molar ratio of 1:0.5] tends to corrode coated aluminium substrates. For Ni–Mo–P (1:0.33)/AA6061 substrate, E_{corr} value could be arranged based on the formation method as follows: electroplating power supply [−452.1 mV] > electroplating chronoamperometry [−491.6 mV] ~ electroless [−493.2 mV]. On the other hand, reduced current density values are shown at AA6061 after its coating with Ni–P and Ni–Mo–P deposits [I_{corr} = 55.1 μA cm^{-2} at bare AA6061]. The presence of molybdenum in Ni–Mo–P coatings, formed by electroplating power supply technique, much lowers their corrosion current density values. This situation was reversed for the coatings formed by electroless plating technique, where the increased molybdenum content in the deposition bath would increase I_{corr} value. The best corrosion resistance behaviour was noticed at Ni–P and Ni–Mo–P coated AA6061 substrates, formed by electroplating chronoamperometry technique, as evidenced by the drastic decrease in their I_{corr} values.

When bare AA6061 was coated with Ni–P, the polarization resistance increases by 1.75, 4 and 29.44 times by applying electroplating power supply, electroless and electroplating chronoamperometry techniques, respectively. Moreover, the incorporation of molybdenum in the deposition bath in Ni:Mo molar ratio of 1:0.33 would further increase R_p values, in relation to that of Ni–P coatings, formed by

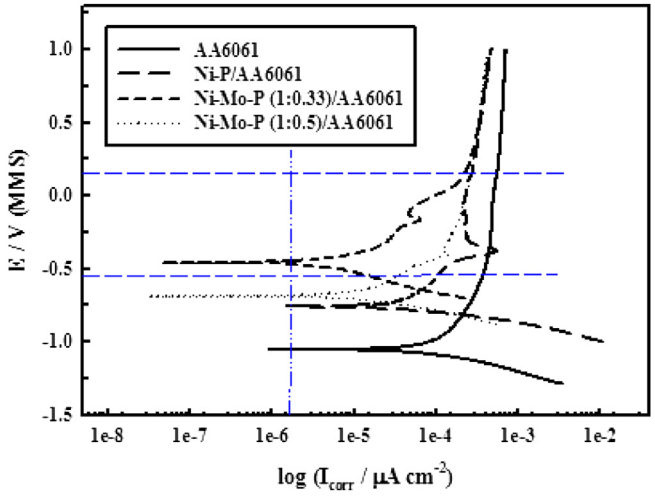

Fig. 3. Potentiodynamic polarization curves of bare and coated AA6061 [by electroplating power supply technique] in (0.5 M H_2SO_4 + 2 ppm HF) solution at 25 °C.

Table 5
Corrosion parameters of AA6061 coated with Ni–P and Ni–Mo–P [in Ni:Mo molar ratios of 1:0.33 and 1:0.5] at 25 °C. These coatings were formed by electroless (a) and electroplating [power supply (b) and chronoamperometry (c)] techniques. The corresponding values of bare AA6061 substrate are inserted in section (a).

Coated substrate	I_{corr}/μA cm^{-2}	$-E_{i=0}$ /mV	β_a/mV	$-\beta_c$ /mV	R_p/Ω cm^2	CR/ mpy
(a)						
Bare AA6061	55.1	1056.0	162.2	79.7	421.5	526.3
Ni–P/AA6061	11.2	610.9	77.0	100.1	1689.5	128.8
Ni–Mo–P (1:0.33)/ AA6061	13.0	493.2	251.6	92.8	2267.4	152.1
Ni–Mo–P (1:0.5)/ AA6061	21.4	723.9	213.2	94.5	1330.3	260.7
(b)						
Ni–P/AA6061	37.2	754.8	330.9	78.2	739.3	427.8
Ni–Mo–P (1:0.33)/ AA6061	3.1	452.1	128.3	133.2	9165.8	36.3
Ni–Mo–P (1:0.5)/ AA6061	4.6	680.5	187.8	95.5	5983.7	56.0
(c)						
Ni–P/AA6061	2.8	670.2	175.6	146.7	12,411.0	32.2
Ni–Mo–P (1:0.33)/ AA6061	1.9	491.6	180.1	134.5	17,619.6	22.2
Ni–Mo–P (1:0.5)/ AA6061	2.6	544.5	124.5	120.8	10,252.7	31.7

different deposition methods. This increase could be arranged in the order: electroless [1.34 times] ~ electroplating chronoamperometry [1.42 times] < electroplating power supply [12.4 times]. However, R_p values would decrease when Ni:Mo molar ratio in the deposition solution is increased to 1:0.5. The corrosion rate of bare AA6061 decreases by 16.34 times after its coating with Ni–P by electroplating chronoamperometry technique [it is 526.3 and 32.2 mpy for bare and coated AA6061, respectively]. On the other hand, Ni–Mo–P (1:0.33)/AA6061 substrate, formed by electroplating power supply method, showed a decreased corrosion rate by 11.79 times, compared to that of the corresponding Ni–P coated Al alloy [it is 427.8 and 36.3 mpy for coated AA6061 with Ni–P and Ni–Mo–P (1:0.33), respectively]. According to the above results, we can conclude that in order to improve the corrosion resistance characteristics of bare AA6061 substrate, it could be coated either with Ni–P by electroplating chronoamperometry technique or Ni–Mo–P (Ni:Mo molar ratio of 1:0.33) by electroplating power supply technique.

Bipolar plate materials should have good corrosion resistance behaviour at an anode potential of −100 mV (SCE) [it equals −540 mV (MMS)] and at a cathode potential of +600 mV (SCE) [it is equivalent to +160 mV (MMS)] [46]. The corresponding current density values at these potentials are listed in Table 6. A corrosion current density of the U.S. DOE (Department of Energy) requirements for bipolar plate materials of PEMFCs is less than 1.6×10^{-6} A cm^{-2} at 2010 and 2015 [47]. Coated AA6061 with Ni–P and Ni–Mo–P by different deposition methods recorded decreased current density values at either anode or cathode potentials by about 10^4–10^6 times, when compared to the U.S. DOE target value. The lowest values were observed at coatings formed by electroplating chronoamperometry technique. Therefore, it is recommended as a good plating method of Al alloy when applied in bipolar plate materials manufacture.

The corrosion performance of Ni–P and Ni–Mo–P coatings is controlled by their elemental weight percentages and surface morphology. The increased corrosion rate of Ni–P deposit is attributed to the prevalence of grooves that allow the corrosive solution penetration [Fig. 2(a)]. Among different preparation methods, Ni–Mo–P (1:0.33) deposit, formed by electroplating power supply technique, contains the highest nickel content [21.97%], lowest P amount [3.69%] and lowest Mo:Ni atomic ratio [0.15:1]. This coating showed a lowered corrosion rate. Melo et al. [48] observed that electrodeposited

Table 6
The related current density values of AA6061 coated with Ni–P and Ni–Mo–P [in Ni:Mo molar ratios of 1:0.33 and 1:0.5] at the potential of anode condition [−540 mV (MMS)] and that of cathode condition [+160 mV (MMS)] as derived from potentiodynamic polarization curves at 25 °C. These coatings were formed by electroless and electroplating [power supply and chronoamperometry] techniques. The corresponding values of bare AA6061 substrate are also inserted.

Coated substrate	I/A cm^{-2}					
	Anode condition [at −540 mV (MMS)]			Cathode condition [at +160 mV (MMS)]		
	Electroless	Power supply	Chronoamperometry	Electroless	Power supply	Chronoamperometry
Bare AA6061	3.74×10^{-10}			5.68×10^{-10}		
Ni–P/AA6061	9.66×10^{-11}	1.08×10^{-10}	1.37×10^{-11}	1.96×10^{-8}	2.78×10^{-10}	5.92×10^{-11}
Ni–Mo–P (1:0.33)/AA6061	3.56×10^{-11}	1.31×10^{-11}	3.66×10^{-12}	2.70×10^{-10}	2.26×10^{-10}	2.05×10^{-11}
Ni–Mo–P (1:0.5)/AA6061	1.12×10^{-10}	3.46×10^{-11}	1.38×10^{-12}	5.35×10^{-10}	2.68×10^{-10}	5.08×10^{-11}

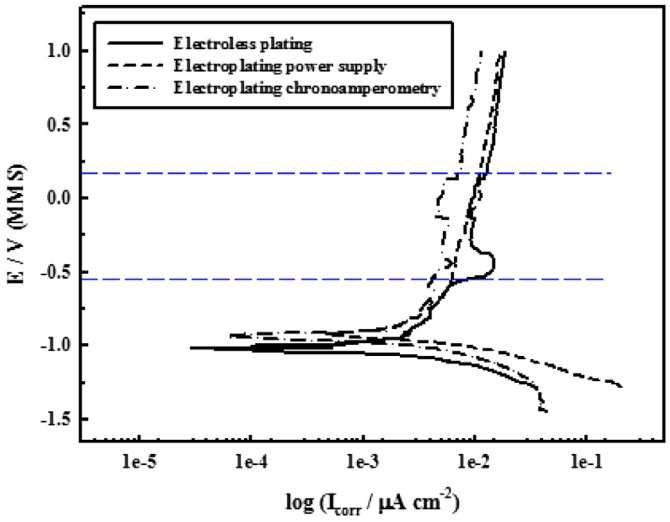

Fig. 4. Potentiodynamic polarization curves of Ni–Mo–P (1:0.33)/AA6061, formed by different deposition methods, in (0.5 M H_2SO_4 + 2 ppm HF) solution at 70 °C.

$Ni_{78}Mo_{10}P_{12}$ amorphous coating presented the best corrosion resistance properties among the prepared alloys. Moreover, the homogeneous nickel distribution all over this coating surface can offer another explanation for its good corrosion resistance behaviour. However, further molybdenum amount increase in the deposition bath [Ni:Mo molar ratio of 1:0.5] would increase the coating roughness and more cracks will appear [Fig. 2(b)]. This may account for its increased corrosion rate as previously observed by Bai et al. [38] who studied the corrosion performance of Ni–Mo–P coating formed by electroless deposition process on aluminium alloy 5052.

The corrosion resistance of Ni–Mo–P (1:0.33)/AA6061 substrate was tested at higher temperature (70 °C). It was formed using different deposition methods. The corresponding polarization curves in (0.5 M H_2SO_4 + 2 ppm HF) solution were shown in Fig. 4. The corrosion parameters were also estimated in Table 7. Much increased I_{corr} values were observed for Ni–Mo–P (1:0.33)/AA6061 substrate at 70 °C, in relation to that at 25 °C. The coated substrate,

Table 7
Corrosion parameters of AA6061 coated with Ni–Mo–P (1:0.33) at 70 °C. These coatings were formed by electroless and electroplating [power supply and chronoamperometry] techniques.

Coating technique	I_{corr}/μA cm^{-2}	$-E_{i=0}$/mV	β_a/mV	$-\beta_c$/mV	R_p/Ω cm^2	CR/mpy
Electroless	4692.2	1082.8	15.2	179.4	1.3	54,898.7
Electroplating power supply	837.7	932.4	192.9	75.4	28.1	9809.5
Electroplating chronoamperometry	1147.0	956.9	285.2	120.0	32.0	13,401.6

Table 8
(a) The related current density values of AA6061 coated with Ni–Mo–P (1:0.33) at 70 °C at the potential of anode condition [−540 mV (MMS)] and that of cathode condition [+160 mV (MMS)] as derived from potentiodynamic polarization curves at 70 °C. These coatings were formed by electroless and electroplating [power supply and chronoamperometry] techniques. (b) The corresponding current density values at chromium nitride coated Al substrates at 70 °C.

(a)

Coating technique	I/A cm^{-2}	
	Anode condition [at −540 mV (MMS)]	Cathode condition [at +160 mV (MMS)]
Electroless	1.00×10^{-8}	1.23×10^{-8}
Electroplating power supply	6.35×10^{-9}	1.13×10^{-8}
Electroplating chronoamperometry	4.19×10^{-9}	7.04×10^{-9}

(b)

Coated substrate	I/A cm^{-2}		Corrosive solution	Reference
	Anode condition [at −540 mV (MMS)]	Cathode condition [at +160 mV (MMS)]		
Al Magnal-45 [Al-5083]	1.92×10^{-3}	1.04×10^{-3}	(0.5 M H_2SO_4 + 2 ppm HF)	[49]
Al–CrN 3 μm	5.48×10^{-5}	1.29×10^{-4}	(0.5 M H_2SO_4 + 2 ppm HF)	[49]
Al–CrN 4 μm	1.89×10^{-5}	1.96×10^{-4}	(0.5 M H_2SO_4 + 2 ppm HF)	[49]
Al–CrN 5 μm	5.74×10^{-5}	7.91×10^{-5}	(0.5 M H_2SO_4 + 2 ppm HF)	[49]
Al–CrN/ZrN	7.32×10^{-5}	9.19×10^{-4}	(1.0 M H_2SO_4 + 2 ppm HF)	[50]

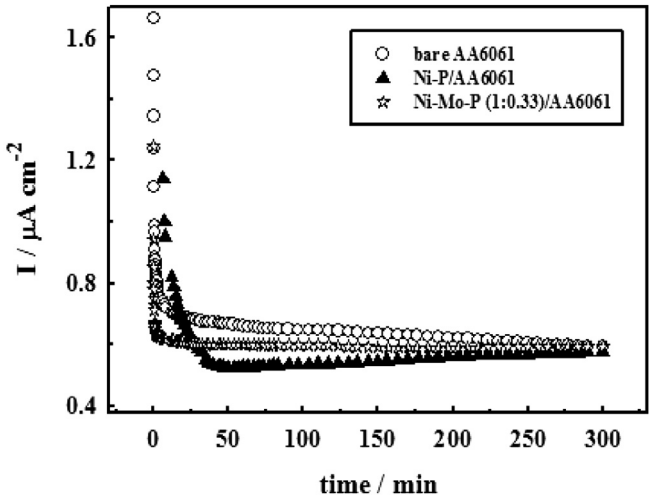

Fig. 5. Potentiostatic polarization curves of bare and coated AA6061 with Ni–P and Ni–Mo–P (1:0.33) at +160 mV (MMS) for 5 h in (0.5 M H_2SO_4 + 2 ppm HF) solution. The coatings were formed by electroplating power supply technique.

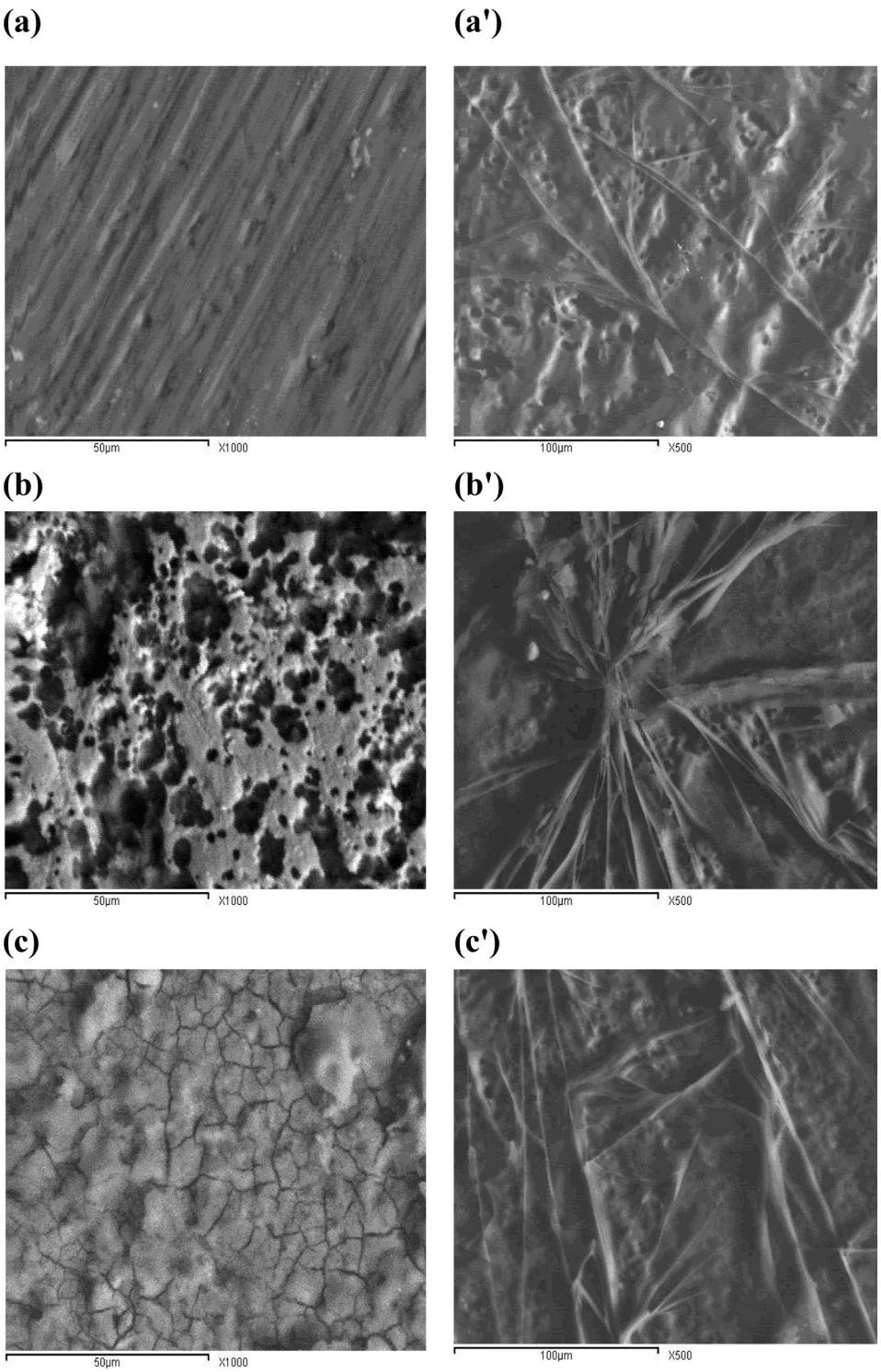

Fig. 6. Scanning electron micrographs of bare (a) and coated AA6061 with Ni–P (b) and Ni–Mo–P (1:0.33) (c) formed by electroplating power supply technique. [(a′), (b′) and (c′)] are those after potentiostatic polarization test for cathode condition in (0.5 M H_2SO_4 + 2 ppm HF) solution at +160 mV (MMS) for 5 h.

using electroplating power supply technique, is the least corroded one [I_{corr} = 837.7 μA cm^{-2}]. On the other hand, applying the electroless deposition method further increases the corrosion current density of coated AA6061 by about 5.6 times. E_{corr} values are also shifted in the negative direction when compared to those at 25 °C. The corresponding current density values of coated AA6061 with Ni–Mo–P (1:0.33) at the potential of anode and cathode conditions as derived from potentiodynamic polarization curves at 70 °C were listed in Table 8(a). These values were found to be lower than those recorded under simulated conditions at chromium nitride coated aluminium substrates at 70 °C by about 10^3–10^4 times [49,50] as shown in Table 8(b). Although the corrosion performance of coated AA6061 with Ni–Mo–P got worse at elevated temperature, Ni–Mo–P deposits are better than comparable coatings.

3.3. Stability of coated AA6061 substrates in simulated cathode condition

The stability of bipolar plate materials during long time operation in polymer electrolyte membrane fuel cells could be measured by applying potentiostatic polarization technique. The cathode working condition was simulated by stepping the potential value at +600 mV (SCE) in air-saturated solution. The corresponding current density–time curves are plotted in Fig. 5 for uncoated and coated AA6061 with Ni–P and Ni–Mo–P (1:0.33) deposits, formed by electroplating power supply technique, at +160 mV (MMS) for 5 h in (0.5 M H_2SO_4 + 2 ppm HF) solution. In general, the current density rapidly decreases at the first few minutes of the polarization test. This accompanies the formation of a passive film at aluminium alloy surface [43,51]. Afterwards, the current density of Ni–Mo–P (1:0.33)/AA6061 is almost stabilized all over the studied period. For Ni–P deposit, a further slight current density increase was shown to infer a corroded surface. After 40 min from beginning of the polarization test, the current density values of uncoated and coated AA6061 substrates could be arranged in an ascending order as follows: Ni–P/AA6061 [0.53 μA cm^{-2}] < Ni–Mo–P (1:0.33)/AA6061 [0.60 μA cm^{-2}] < bare AA6061 [0.67 μA cm^{-2}]. Therefore, Ni–P deposit is more stable than Ni–Mo–P after a relatively short time. However, at the end of the polarization experiment [after 5 h], the current density of the three studied substrates is almost the same.

The surface morphology of uncoated and coated AA6061 with Ni–P and Ni–Mo–P (1:0.33) deposits, formed by electroplating power supply technique, before and after potentiostatic polarization test at +160 mV (MMS) in (0.5 M H_2SO_4 + 2 ppm HF) solution for 5 h is represented in Fig. 6. Although the surface morphology of bare AA6061, Ni–P and Ni–Mo–P coated substrates before polarization is completely different, they nearly share in one morphology image after the stability test. The surface of Al alloy appears as a tree with many branches. Numerous pits are distributed along aluminium substrate. The density of these grooves is somewhat evident at bare AA6061 surface to conclude for its higher corrosion rate. The dense molybdenum oxide film formed on Ni–Mo–P coated surface would improve its long-term corrosion resistance [52,53]. Passive Mo element could accumulate on the grain boundaries to stuff the grooves in Ni–Mo–P coating [36,54], thus preventing the diffusion of the corrosive media through them.

3.4. Interfacial contact resistance measurements of coated AA6061 substrates

The interfacial contact resistance values between coated AA6061 substrates and carbon paper were measured at different compaction forces in Fig. 7. This study was carried out at uncoated and coated AA6061 substrate with Ni–P and Ni–Mo–P (1:0.33) deposits formed by electroplating power supply technique. The interfacial contact resistance values of bare AA6061 substrate gradually decrease with increasing the compaction force. This is a result of the increased contact area with increasing pressure till a nearly stable ICR value is measured [55,56]. The formed oxide layer at bare AA6061 surface increases its electrical resistivity. This may rationalize the increased ICR values at uncoated substrate when compared to coated ones. After coating AA6061 with Ni–P and Ni–Mo–P, ICR values decrease by 2.22 and 1.88 times, respectively at a compaction force value of 140 N cm^{-2}. The presence of nickel and molybdenum would decrease the electrical resistivity of Ni–P/AA6061 and Ni–Mo–P/AA6061 substrates [57]. Wang et al. [58] have attributed the decreased ICR value at molybdenum nitride modified AISI 304 stainless steel to the higher conductivity of the coating prepared by plasma surface diffusion alloying method. A

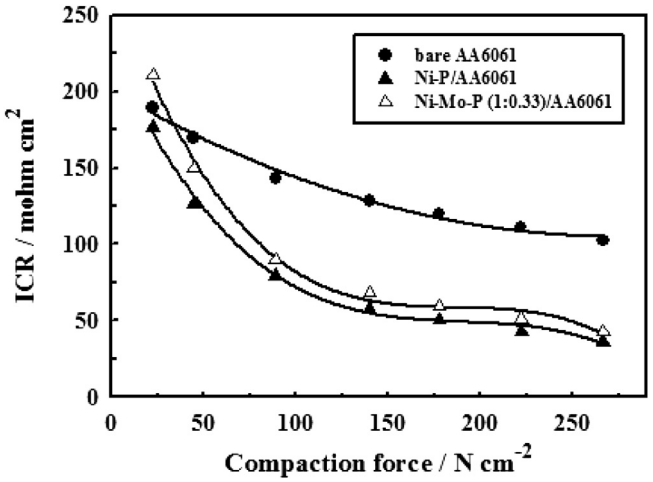

Fig. 7. Variation of interfacial contact resistance of bare and coated AA6061 with Ni–P and Ni–Mo–P (1:0.33) with compaction force. These coatings were formed by electroplating power supply technique.

Table 9
ICR values at 140 N cm^{-2} for different aluminium-based substrates.

Substrate	ICR/mΩ cm^2	Reference
Bare pure Al	257.25	[34]
Bare Al alloy 1050 [AA1050]	351.75	[34]
Bare Al alloy 3004 [AA3004]	311.25	[34]
Bare Al alloy 5251 [AA5251]	211.25	[33]
Ni–P/AA5251	150.75	[33]
Ni–Co–P/AA3004	209.25	[34]
Ni–Co–P/pure Al	142.35	[34]
Ni–Co–P/AA5251	114.45	[33]
Ni–Co–P/AA6061	77.75	[34]

list of ICR values at 140 N cm^{-2} for different aluminium-based substrates is represented in Table 9. With regarding the values in this table, our prepared samples in the present work still showed lower ICR values. Therefore, coating AA6061 with Ni–P and Ni–Mo–P improves its interfacial contact resistance with the gas diffusion layer.

4. Conclusion

1. Metals offer a number of design advantages, particularly for automotive stack applications, including: low-cost; mass-production via stamping or embossing of sheet products; fabrication into very thin forms (<150 mm) to reduce weight and volume in the overall stack; impermeability to fuel, oxidant and water vapour; and in general, excellent thermal conduction properties and good mechanical robustness [59]. The application of coated aluminium substrates as bipolar plate materials tends to reduce PEMFCs cost. Tawfik et al. [46] have studied a cost comparison on using graphite and treated aluminium bipolar plates and showed that after the first 6 months of operation, the total cost of graphite composites begins to exceed the metallic bipolar plates.
2. Ni–P and Ni–Mo–P coatings were formed on AA6061 by electroless and electroplating techniques.
3. Scanning electron microscopy showed a coarse Ni–Mo–P coating with bright nickel deposits. Many cracks were observed.
4. The atomic percentage of molybdenum to nickel was varied in Ni–Mo–P (1:0.33) coating based on the formation method. It increases in the order: electroplating power supply [0.15:1] < electroplating chronoamperometry [0.74:1] < electroless [1.39:1].

5. As the amount of Na_2MoO_4 in the plating solution increases, less phosphorous will be deposited.
6. Coating AA6061 with Ni–P using electroplating chronoamperometry technique decreases its corrosion rate by 16.34 times. Adding molybdenum to Ni–P/AA6061 in Ni:Mo molar ratio of 1:0.33 by electroplating power supply method increases its polarization resistance by 12.4 times.
7. The current density values of Ni–P and Ni–Mo–P coated aluminium substrate at either anode or cathode potentials decreased by about 10^4–10^6 times, relative to the U.S. DOE target value.
8. The high electrical conductivity of nickel and molybdenum could account for the decreased ICR values of Ni–P and Ni–Mo–P coated substrates.

References

[1] R. Tian, J. Sun, Int. J. Hydrogen Energy 36 (2011) 6788–6794.
[2] C. Du, P. Ming, M. Hou, J. Fu, Q. Shen, D. Liang, Y. Fu, X. Luo, Z. Shao, B. Yi, J. Power Sources 195 (2010) 794–800.
[3] D.P. Davies, P.L. Adcock, M. Turpin, S.J. Rowen, J. Appl. Electrochem. 30 (2000) 101–105.
[4] D.R. Hodgson, B. May, P.L. Adcock, D.P. Davies, J. Power Sources 96 (2001) 233–235.
[5] J. Jayaraj, Y.C. Kim, K.B. Kim, H.K. Seok, E. Fleury, Sci. Technol. Adv. Mater. 6 (2005) 282–289.
[6] S.-J. Lee, C.-H. Huang, Y.-P. Chen, Y.-M. Chen, J. Fuel Cell Sci. Technol. 2 (2005) 208–212.
[7] S.-J. Lee, C.-H. Huang, Y.-P. Chen, J. Mater. Process. Technol. 140 (2003) 688–693.
[8] D.E. Tallman, M.P. Dewald, C.K. Vang, G.G. Wallace, G.P. Bierwagen, Curr. Appl. Phys. 4 (2004) 137–140.
[9] R.L. Borup, N.E. Vanderborgh, Mater. Res. Soc. Symp. Proc. 393 (1995) 151–155.
[10] V. Mehta, J.S. Cooper, J. Power Sources 114 (2003) 32–53.
[11] A. Hermann, T. Chaudhuri, P. Spagnol, Int. J. Hydrogen Energy 30 (2005) 1297–1302.
[12] Y. Wang, D.O. Northwood, J. Power Sources 165 (2007) 293–298.
[13] I.E. Paulauskas, M.P. Brady, H.M. Meyer III, R.A. Buchanan, L.R. Walker, Corros. Sci. 48 (2006) 3157–3171.
[14] E.A. Cho, U.-S. Jeon, S.-A. Hong, I.-H. Oh, S.-G. Kang, J. Power Sources 142 (2005) 177–183.
[15] H. Wang, M.P. Brady, K.L. More, H.M. Meyer III, J.A. Turner, J. Power Sources 138 (2004) 79–85.
[16] H. Wang, M.P. Brady, G. Teeter, J.A. Turner, J. Power Sources 138 (2004) 86–93.
[17] Y.J. Ren, C.L. Zeng, J. Power Sources 171 (2007) 778–782.
[18] S. Joseph, J.C. McClure, P.J. Sebastian, J. Moreira, E. Valenzuela, J. Power Sources 177 (2008) 161–166.
[19] J. Hu, Y.B. Li, H.L. Wang, W.C. Ren, Mater. Lett. 62 (2008) 1715–1717.
[20] M.N. Hull, J. Electroanal. Chem. 38 (1972) 143–157.
[21] M.N. Hull, J. Electroanal. Chem. 30 (1971) App. 1–App. 3.
[22] J.W. Johnson, C.H. Chi, C.K. Chen, W.J. James, Corrosion 26 (1970) 238–242.
[23] J.W. Johnson, M.S. Lee, W.J. James, Corrosion 26 (1970) 507–510.
[24] L.L. Wikstrom, K. Nobe, J. Electrochem. Soc. 116 (1969) 525–530.
[25] J. Besson, G. Drautzburg, Electrochim. Acta 3 (1960) 158–168.
[26] W.A. Badawy, F.M. Al-Kharafi, Electrochim. Acta 44 (1998) 693–702.
[27] W. Baoxing, D. Shaojun, J. Electroanal. Chem. 379 (1994) 207–214.
[28] S. Liu, B. Wang, B. Liu, S. Dong, Electrochim. Acta 45 (2000) 1683–1690.
[29] T.S.N. Sankara Narayanan, S.K. Seshadri, J. Alloys Compd. 365 (2004) 197–205.
[30] M. Palaniappa, S.K. Seshadri, J. Mater. Sci. 42 (2007) 6600–6606.
[31] K.H. Krishnan, S. John, K.N. Srinivasan, J. Praveen, M. Ganesan, P.M. Kavimani, Metall. Mater. Trans. A 37 (2006) 1917–1926.
[32] R.C. Agarwala, V. Agarwala, Sadhana 28 (2003) 475–493.
[33] A.E. Fetohi, R.M. Abdel Hameed, K.M. El-Khatib, E.R. Souaya, Int. J. Hydrogen Energy 37 (2012) 7677–7688.
[34] A.E. Fetohi, R.M. Abdel Hameed, K.M. El-Khatib, E.R. Souaya, Int. J. Hydrogen Energy 37 (2012) 10807–10817.
[35] D. Ferdous, A.K. Dalai, J. Adjaye, Appl. Catal. A Gen. 260 (2004) 137–151.
[36] Y. Wu, C.C. Wan, Y.Y. Wang, J. Electron. Mater. 34 (2005) 541–550.
[37] G. Lu, G. Zangari, J. Electrochem. Soc. 150 (2003) C777–C786.
[38] C.-Y. Bai, Y.-H. Chou, C.-L. Chao, S.-J. Lee, M.-D. Ger, J. Power Sources 183 (2008) 174–181.
[39] K. Azumi, T. Yugiri, M. Seo, K. Tashiro, S. Kawashima, Hyomen Gijutsu 51 (2000) 313–318.
[40] K. Azumi, Y. Fujishige, M. Seo, L. Nanis, H. Nakao, K. Tashiro, Hyomen Gijutsu 48 (1997) 1019–1024.
[41] K. Azumi, Y. Fujishige, M. Seo, L. Nanis, H. Nakao, K. Tashiro, Hyomen Gijutsu 47 (1996) 802–807.
[42] S.-W. Tang, C.-J. Wang, Y.-L. Sun, J. Hu, Surf. Coat. Technol. 205 (2010) 43–49.
[43] H. Wang, M.A. Sweikart, J.A. Turner, J. Power Sources 115 (2003) 243–251.
[44] M.C. García-Alonso, M.L. Escudero, V. López, A. Macías, Corros. Sci. 38 (1996) 515–530.
[45] H.-S. Yu, S.-F. Luo, Y.-R. Wang, Surf. Coat. Technol. 148 (2001) 143–148.
[46] H. Tawfik, Y. Hung, D. Mahajan, J. Power Sources 163 (2007) 755–767.
[47] The Hydrogen, Fuel Cells & Infrastructure Technologies Program Multi-year Research, Development and Demonstration Plan, Department of Energy, Washington, DC, US, February 2005, pp. 3–89. http://www1.eere.energy.gov/hydrogenandfuelcells/mypp/pdfs/fuel_cells.pdf.
[48] R.L. Melo, P.N.S. Casciano, A.N. Correia, P. de Lima-Neto, J. Braz. Chem. Soc. 23 (2012).
[49] J. Barranco, F. Barreras, A. Lozano, M. Maza, J. Power Sources 196 (2011) 4283–4289.
[50] J. Barranco, F. Barreras, A. Lozano, A.M. Lopez, V. Roda, J. Martin, M. Maza, G.G. Fuentes, E. Almandoz, Int. J. Hydrogen Energy 35 (2010) 11489–11498.
[51] M. Kumagai, S.-T. Myung, S. Kuwata, R. Asaishi, H. Yashiro, Electrochim. Acta 53 (2008) 4205–4212.
[52] Y. Gao, Z.J. Zheng, M. Zhu, C.P. Luo, Mater. Sci. Eng. A 381 (2004) 98–103.
[53] H. Lou, S. Zhu, F. Wang, Oxid. Met. 43 (1995) 317–328.
[54] M.-A. Nicolet, Thin Solid Films 52 (1978) 415–443.
[55] L. Zhang, Y. Liu, H. Song, S. Wang, Y. Zhou, S.J. Hu, J. Power Sources 162 (2006) 1165–1171.
[56] S. Rudenja, C. Leygraf, J. Pan, P. Kulu, E. Talimets, V. Mikli, Surf. Coat. Technol. 114 (1999) 129–136.
[57] Y.-H. Chou, Y. Sung, Y.-M. Liu, N.-W. Pu, M.D. Ger, Surf. Coat. Technol. 203 (2009) 1020–1026.
[58] L. Wang, J. Sun, P. Li, J. Sun, Y. Lu, B. Jing, S. Li, S. Ji, Z. Wen, Int. J. Hydrogen Energy 37 (2012) 5876–5883.
[59] B.-C. Cha, Y.-Z. You, S.-T. Hong, J.-H. Kim, D.-W. Kim, B.-S. Lee, S.-K. Kim, Int. J. Hydrogen Energy 36 (2011) 4565–4572.